Dynamic Light Scattering of Polymer/Solvent Solutions Under Pressure. Near-Critical Demixing (0.1 < *P*/MPa < 200) for Polystyrene/Cyclohexane and Polystyrene/Methylcyclohexane

W. Alexander Van Hook,* Hannah Wilczura,† and Luis P. N. Rebelo‡

Chemistry Department, University of Tennessee, Knoxville, Tennessee 37996

Received February 18, 1999; Revised Manuscript Received August 7, 1999

ABSTRACT: A conveniently sized high-pressure scattering cell used for 90° DLS (dynamic light scattering) measurements on polymer solutions is described (0 < *P*/MPa < 200; 283 < *T*/K < 373). DLS parameters are reported for semidilute solutions of polystyrene (PS) of various molecular weight in Θ-solvents (cyclohexane (CH) and methylcyclohexane (MCH)), above and below T_Θ, and at high enough concentration to ensure that precipitation, when it occurs, follows spinodal decomposition/percolation. In the homogeneous region, close to and above T_Θ, the correlograms, initially monomodal and diffusive, split at high pressure. The intensity and the correlation radius of the diffusive mode diverge as critical demixing is approached during pressure or temperature quenches. That process is described in the $(T,P)_{\psi cr}$ plane using a multidimensional reduced scaling formalism developed for the purpose. The analysis of the scattering and the phase equilibrium data for PS/CH is complicated by the pressure dependence of the CH freezing curve, but that for PS/MCH nicely exemplifies behavior across a good part of the $(T,P)_{\psi cr}$ reentrant miscibility island showing multiple hypercritical points. It has been discussed in that context.

1. Introduction

This laboratory has reported on liquid−liquid demixing from solutions of polystyrene (PS) in various small-molecule solvents over broad ranges of temperature and pressure, isotope label (H/D) on solute or solvent, polymer concentration, molecular weight, and polydispersity.[1−5] The solutions display upper and lower two-phase consolute branches, (UCS and LCS respectively), which join at hypercritical points which are themselves temperature, pressure, isotope, and molecular weight dependent. The data have been interpreted using a mean field algorithim based on a continuous thermodynamic modification of Flory−Huggins theory[3] or (alternatively) with a scaling model which correlates the demixing parameters with a number of variables, including commonly employed solvent quality indices.[6] More recently, we have turned attention from the purely phenomonological thermodynamic description of the loci of the phase transitions to more detailed studies which include the mechanism of the precipitation. The newer studies employ dynamic light scattering (DLS) to compare those regions of the phase diagram where demixing occurs via nucleation/growth (NG), with demixing at higher concentration via spinodal decomposition (SD).[7,8] The transitions were induced by thermal quenching. In this paper we broaden the approach and report DLS studies during pressure quenches of PS/cyclohexane (CH) and PS/methylcyclohexane (MCH) solutions in the range (0.1 < *P*/MPa < 200) at temperatures as high as 373 K. We have been particularly interested in comparing fast-mode dynamic correlation radii and intensities obtained from DLS measurements, ξ^f and I^f, inside the homogeneous one-phase region with those properties at and beyond the Θ conditions near temperature-quench or pressure-quench induced phase separation (i.e. to the poor solvent side). Thus, in this study we are interested in determining ξ^f near the LL phase transition as a function of the direction of approach to demixing (especially in the region close to hypercritical points), and in extending the (P,T) range of the measurements in an attempt to locate $P_{hyp}{}^U$ and $T_{hyp}{}^U$, should they exist. In preliminary reports we outlined DLS results for PS/MCH (0 < *P*/MPa < 50) near room temperature and compared with small-angle neutron scattering (SANS).[9,10]

Brown and Nicolai[11] and Berry[12] have reviewed DLS measurements on semidilute polymer solutions in good solvents (e.g., toluene, benzene, etc.), and in Θ solvents. The solvents in this study, CH and MCH, are both Θ solvents, and CH is a significantly better solvent than MCH (Θ_{UCS}(CH) = 307 K, Θ_{LCS}(CH) = 486 K, and Θ_{UCS}(MCH) = 345 K, Θ_{UCS}(MCH) = 465 K, both at P = 0.1 MPa).[6] Solutions in good solvents have been thoroughly studied. At 0.1 MPa and low enough molecular weight, DLS correlograms are well described in terms of a single (monomodal) exponential decay, $g_1(t) = B\exp(-\Gamma t)$. This permits definition of a correlation radius, ξ, obtained from the cooperative diffusion coefficient of the system, $D = \Gamma/q^2$, using eq 1. k_B is Boltzmann's constant, η_o the

$$\xi = k_B T/(6\pi\eta_o D) \qquad (1)$$

solvent viscosity, and $q = (4\pi/\lambda)\sin(\theta/2)$ with λ the radiation wavelength and θ the scattering angle. In the low-concentration, low-pressure limit, ξ approaches the hydrodynamic radius ξ_h. Low pressure correlograms in Θ solvents are often more complex. As concentration increases, the initially simple exponential form changes shape to a more complicated bimodal pattern. The first component, a narrow peak found at shorter time, varies linearly with q^2 and is clearly diffusive in nature. The slow peak, important only at concentrations above

* To whom correspondence should be addressed.

† On leave at the University of Tennessee, 1996−1998. Permanent address: Chemistry Department, University of Warsaw, Pasteura 1, 02-089 Warsaw, Poland.

‡ On leave at the University of Tennessee, 1996-1997. Permanent address: Chemistry Department, New University of Lisbon, 2825 Monte da Caparica, Portugal.

10.1021/ma990238b CCC: $18.00
Published on Web 09/30/1999

Table 1. Characteristics of Polystyrene Samples

polymer	M_w/amu	M_w/M_n	source[a]
PS30K	30 000	<1.06	PC-80317
PS90K	90 000	<1.04	PC-50522
PS400K	400 000	<1.06	PC-00507

[a] PC = Pressure Chemical followed by lot no.

entanglement, broadens with increasing molecular weight and concentration as its average position shifts toward longer time. Hydrodynamic correlation lengths are determined from the parameters defining the short time decay.[11] The longer time relaxation process has heretofore only been observed for polymer solutions of reasonably high concentration and MW. By performing q-dependent temperature-quench experiments on both PS/CH and PS/MCH solutions over broad concentration ranges, Szydlowski and Van Hook[7,8] confirmed the faster relaxation process to be diffusive and the slower nondiffusive. In the material which follows, we assume that conclusion holds in the region of pressure-quench induced precipitation. The authors[7,8] also discussed complications due to multiple scattering. These matters are treated in more detail in a later section.

DLS measurements at elevated pressure are inconvenient and we have found previous measurements from just a few groups. Fytas, Patkowski, Meier, and Dorfmuller[13−15] studied acrylate polymers at near ambient temperature ($0.1 < P/\text{MPa} < 210$). More recently Smith, Freeman and Hall[16] reported measurements on low MW polypropylene oxide near the glass transition at 253 K ($250 < P/\text{MPa} < 390$). To our knowledge the present data represent the first DLS measurements on polymer solutions in the vicinity of pressure induced demixing, although Kiepen and Borchard,[17] Steinhoff, Rullmann, Kuhne, and Alig,[18] and Xiong and Kiran[19] have described cells used for static light scattering of polymer solutions during pressure induced precipitation ($0 < P/\text{MPa} < \sim 80$), and Lechner and Mattern[20] reported static and dynamic light scattering measurements on poly(vinyl alcohol)/water/alcohol solutions at high pressure and temperature, but not in the vicinity of the phase transition.

2. Experimental Section

Materials and Sample Preparation. High-purity polystyrene samples of low polydispersity were purchased from Pressure Chemical Co. and are specified in Table 1. Reagent cyclohexane (CH) and methylcyclohexane (MCH or MCHh) and perdeuteromethylcyclohexane (MCHd) were purchased from Aldrich Chemical and used as received except for drying over molecular sieves and filtration through poly(tetrafluoroethylene) (0.2 μm) (Alltech or Whatman).

Dynamic Light Scattering. DLS measurements were made using a Bookhaven Instruments Corp. package which included a BI-200SM goniometer, BI-9025AT correlator, EMI B2FBK/RMI photomultiplier, Spectraphysics model 127 50 mw He−Ne laser, and software package with single and double exponential, CUMULANT, and CONTIN data analysis. The present measurements were limited to $\theta = 90$.

The Pressure Cell. DLS measurements were performed using one of a series of high-pressure optical cells, Figure 1. It has been used to 200 Ma and 373 K and is designed to fit the goniometer without modification of the instrument or the optical path. The stainless steel cell body (35 mm in height; 27 mm in diameter) encloses a "T"-shaped 90° optical path. Each 2.5 mm leg ending at a sapphire window (6.3 mm diameter × 3.2 mm) is seated on a 6.25 mm polished shoulder and gasketed to either side with annealed and polished soft copper gaskets. Window-gasket assemblies are held in place

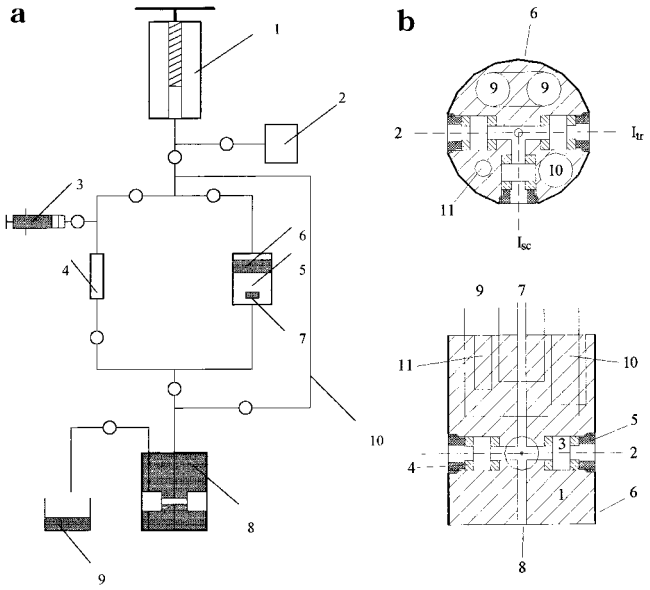

Figure 1. Schematic of high-pressure DLS scattering cell and the sample handling and pressure generating system. (a, left) Pressure generating and sample handling system. Key: (1) motor driven pressure generator; (2) pressure gauge [then using the left path with solutions prepared at 0.1 MPa]; (3) hypodermic for sample injection at $P \sim 0.1$ MPa; (4) buffer volume, [**or** using the right path]; (5) mixing chamber for solution preparation at $P > 0.1$ MPa; (6) Teflon separator; (7) magnetic stirrer; (8) high pressure DLS cell; (9) waste. Valves symbolized by "○". The outermost path, "10", permits independent pressurization of the scattering cell while the solution is being prepared in mixing chamber 5. (b, right top) Top view of scattering cell with incident (2), transmitted (I_{tr}) and scattered beams (I_{sc}), and approximate locations of path to circulate thermostatting fluid (9), and sample (7), and auxiliary heater (10) and thermometer (11) wells. (b, right bottom) Side view of scattering cell (35 mm height, 27 mm diameter): (1) cell body; (2) optical path; (3) sapphire windows; (4) copper gaskets; (5) cap screws; (6) Teflon sleeve; (7) sample entrance; (8) sample exit; (9) thermostating fluid: (10) auxiliary electrical heater well; (11) thermometer well.

with hardened steel capscrews torqued to ~30 ft-lbs. Careful attention is necessary to prevent scratching and shattering the windows under the resulting high stress. During an experiment the cell sits on a thin Teflon pad resting on the bottom of the RI-matching-fluid reservoir. It is cased in a Teflon sleeve (except windows), which provides convenient centering and a modicum of insulation between cell and goniometer housing.

Sample enters and leaves via a 1/16 in. path drilled along the centerline and fitted top and bottom to 1/16 in. stainless tubing. Entrance and exit lines are closed with 1/16 in. valves and lead via a solution reservoir to the pressure generator or to waste. Because of space limitations the exit line turns sharply within a slot at the base and rear and exits parallel to the inlet. With this design the sample cavity can be cleaned and flushed while in place in the scattering chamber. This important convenience contributes to the success of the design. Thermostating fluid is circulated through a $^1/_4$ in. diameter "U" shaped hole in the cell body, and supplemental resistance heating is sited in another $^1/_4$ in. hole. Temperature is measured with a 100 Ω RTD platinum resistance thermometer (Omega Engineering) in a $^1/_8$ in. diameter well. The pressure generator is similar to one previously described by us.[21] Pressure is monitored using a 0.01% precision electrical transducer (Precise Sensors, Inc., Monrovia CA, model 6550).

Comments on Window Design. For DLS measurements of acceptable quality, it is necessary to scrupulously filter samples or other fluids placed in the light path and to carefully avoid spurious reflections from window imperfections, window surfaces, cell walls, and other places. Our initial attempts used

Table 2. Smoothing Relations for Viscosity for Cyclohexane and Methylcyclohexane

MCH_{14} (ref 23)	$\eta_{(0.1MPa)} = 7.0063 - 0.0339T + 4.2656 \times 10^{-5}T^2$
CHh_{12} (ref 24)	$\eta_{(0.1MPa)} = 12.9138 - 0.0671T + 8.976 \times 10^{-5}T^2$
MCH and CH (ref 25)	$\log(\eta_p/\eta_{0.1MPa}) = [3.6367 \times 10^{-3} - 1.12 \times 10^{-5}(t - 30)](p) + [-8.7347 \times 10^{-7} + 5.3910 \times 10^{-9}(t - 30)](p)^2$
$\eta(d_{12})/\eta(h_{12}) = 1.06$ (ref 26)	

units: η = centipoises; t = °C T = K; p = MPa

sapphire capillary following an early design,[1,21] but these attempts failed as we were unable to find an affordable capillary of sufficient quality for DLS. This is because the refractive index of sapphire is too high to allow RI matching at the high curvature (small sample) required at pressures of interest. Stray reflection is exacerbated at high curvature. Flat windows of acceptable quality are easier to obtain and are more economical. This rationalizes the present design.

Operation. To begin an experiment, the cell was filled with clarified solvent and background measured. Polymer solution was injected using a hypodermic syringe fitted with a clarifying filter, displacing solvent from the capillary line and buffer volume and from the cell itself (Figure 1, left). Pressure is applied via hydraulic lines (normally solvent is used as the pressurizing fluid), but the sample/solvent interface remains in the capillary connecting line between the buffer volume and pressure generator, or at the highest pressures, in the buffer volume itself which is sized to allow for compression of the solution (as much as ∼10%) in order to keep the solvent/solution interface a safe distance from the scattering cell. Often solvent quality is enhanced by pressure and in some experiments we studied solutions which are demixed at 0.1 MPa at accessible temperatures. In those cases a mixing/sample-preparation chamber separated from the pressure generator with a Teflon plug was placed in the line just above the pressure cell. The mixing chamber, charged with a proper amount of polymer and clarified solvent, is pressurized, heated, and stirred to effect solution, after which the solution, still under pressure, can be injected into the scattering cell by displacing pressurized solvent (Figure 1a).

Toluene RI Matching (Pro and Con). Early in the program we employed a thermostated toluene bath (±∼0.01 K) for refractive index matching and temperature control. At elevated temperature, however, we found DLS data quality to deteriorate due to RI striations in the matching fluid caused by thermal fluctuations. That difficulty prompted a series of measurements without matching fluid. We were surprised to find little or no deterioration in data quality near room temperature and decided improvement at elevated temperature. For the present polymer solutions, (easily studied due to high scattering intensity), results with and without RI matching are essentially equivalent, at least for our purpose which is to study trends in ξ and I as LL demixing is approached by T or P quenches.[22]

Viscosity. Solvent viscosities were obtained from standard sources[23−26] and smoothed by least-squares methods. Smoothing relations are reported in Table 2.

Results and Discussion

The Pressure Dependence of the Correlation Function in a Θ Solvent. A relatively small number of DLS studies have been reported on semidilute solutions at T_Θ and below, presumably because the complexity of the correlograms in that region makes interpretation difficult. Brown and Nicholi[11] and Berry[12] have reviewed the available information for DLS of high MW PS solutions near T_Θ in interesting detail. They find an approximately bimodal distribution associated with fast and slow modes. A narrow peak at short time varies linearly with q^2, is diffusive in nature, and is assigned to the cooperative diffusion coefficient of the transient gel (and associated correlation radius) used to describe the network of entanglement interactions in semidilute polymer solutions (D and ξ^f). The slow mode is more difficult to interpret. At 0.1 MPa it broadens with increasing MW or concentration and its average position shifts to longer times. The authors comment that the general features are in agreement with the Brochard−deGennes model of semidilute polymer solutions,[27,28] if one assumes that the disentanglement of the transient network is characterized not by a single relaxation time but by a broad range of relaxation times. Thus, in the context of the theoretical analysis of Adam and Delsanti,[29] Brown and Nicholai[11] interpret the slow q-independent peak in terms of viscoelastic modes associated with polymer entanglements. (Semenov,[30] Doi and Onuki,[31] and Genz[32] have offered further refinements of the theory). Sun and Wang,[33] on the other hand, maintain that polymer entanglement is not a prerequisite for the appearance of the viscoelastic modes, although it is expected to enhance the slow mode in the DLS spectrum. In first order, for solutions not too close to near-critical precipitation, one expects the DLS spectrum to exhibit an appreciable pressure coefficient (because solvent and hence solution viscosity increases exponentially with pressure). For the entanglement interpretation, on the other hand, we anticipate little or no pressure dependence. It is in this context that experiments of the kind described in this paper may eventually become of interest in distinguishing between the two interpretations. Unfortunately, until the slow mode found at high pressure is better characterized (i.e., by determining the q dependence and comparing it with the longest chain relaxation times) the issue remains unresolved.

Comments: In this part of the paper we compare fast and slow DLS relaxation times, Γ^f and Γ^s, and the relative contributions of the fast and slow modes to the CONTIN distributions, I^f and I^s, for PS/CH, PS/$MCHh_{14}$ and PS/$MCHd_{14}$ solutions of several molecular weights for ($0.1 < P/MPa < 200$) and ($21 < t/°C < 85$). Because of space constraints on window placement in the high-pressure optical cell (vide supra) the present scattering data are limited to 90°, i.e. the q dependence could not be investigated. For that reason comparison with the earlier studies[7,8] which include measurements of the q dependence of scattering in the neighborhood of T-quench induced precipitation is important. In comparing the qualitative features of the scattering data in this paper (P- and/or T-quench) with the earlier[7,8] T-quench data we find no difference in the character of the plots of scattering data vs quench coordinate for the approach to precipitation along either path (i.e. T- or P-quench, using appropriately reduced coordinates[9,10]). On the basis of that observation, and for convenience in comparing the present fast-mode data with other studies, we have chosen to report the present data as reduced and weighted reciprocal relaxation times, $(1/\Gamma_{90})_{red} = (kTq_{90}^2)/(6\pi\eta\Gamma)$ (Tables 1 and 2, Supporting Information). Earlier q-dependent measurements on the same solutions at 0.1MPa,[7,8] showed the Γ^f mode (but not Γ^s) to be diffusive (i.e. Γ^f proportional to q^2) confirming the observations of Brown and Nicholai,[11] $(1/\Gamma^f_{0.1MPa})_{red} = \xi^f_{(0.1)}$. If, as seems reasonable, the diffusive character of

the fast mode persists to high pressure at useful approximation, then $(1/\Gamma^{f}_{P})_{red} \sim \xi^{f}_{(P)}$. We employ that assumption (or simplification in notation, if you will) to set the stage for the discussion of fast mode contributions which follows, and to enable comparisons of the present DLS measurements with static correlation radii obtained by small-angle neutron or light scattering.[9,10,34] More careful comparisons will require q-dependent DLS measurements on pressurized solutions.

An additional difficulty introduced by the window design constraint which limits the measurements to $\theta = \pi/2$, $q = 0.014$ nm^{-1}, is the confusion which arises from the complicated q dependence theoretically expected close to the critical demixing locus. According to mode-coupling theory developed by Kawasaki and Lo[35] and reviewed by Stepanek,[36] the critical contribution to the decay rate is such that $\Gamma(q)/q^2 \sim$constant ($=\xi^{-1}$) in the limit of $(q\xi) \ll 1$, crossing in the approximate vicinity of $(q\xi) \sim 1$ to $\Gamma(\theta)/q^3 \sim$ constant (independent of ξ^{-1}) in the other limit ($q\xi \gg 1$). Fortunately the bulk (63%) of the data presented in the Supporting Information, Tables 1 and 2, lie below $(q\xi) = 1$, almost all (83%) lie below or are in the crossover region (i.e. are below $q\xi = 2$), and only very few (3%) lie at or above $q\xi = 5$. With that in mind, we feel the present method of data handling, while approximate, is appropriate.

Another issue of concern is that DLS data in the region of interest to are subject to distortion by multiple scattering and, for polymer solutions, possible nonequilibrium effects. These matters are discussed in Chapters 6, 14, and 16 of ref 11. Although the effects of multiple scattering may be reduced or eliminated by refractive index matching of solute and solvent, that is not the situation in the solutions under study. Multiple scattering can distort the intensity correlation function to such an extent that in extreme cases the precipitation or preprecipitation character of the solution cannot be quantitatively interpreted in terms of physically meaningful ξ's. Even so, as we commented in the earlier study,[7] "fast-mode correlation lengths calculated from the observed autocorrelation functions with no concern for multiple scattering corrections appear qualitatively the same as those obtained from low intensity measurements during early stages (i.e. in the absence of multiple scattering). Even though ... the scattering intensity (and its q-dependence[7]) increases dramatically near the point of precipitation, changes in the autocorrelation function are modest, it is relatively well behaved. Unfortunately presently available software does not include corrections for multiple scattering and/or other interference effects."

In the vicinity of critical demixing the concentration fluctuation dynamics monitored by DLS slow; it therefore becomes important to ensure that equilibrium is well established before scattering intensities are recorded. It is for that reason the present P-quench technique was carried out stepwise (i.e. changing P, waiting for equilibrium, and finally recording I_{sc}). That technique was also demanded by the thermal relaxation time of the pressure cell returning to its control temperature following adiabatic cooling (or heating). Rapid (~adiabatic) pressure changes lead to appreciable cooling (or heating). Usually a several minute delay was sufficient to reestablish thermal stability and to ensure a stable and unchanging scattering intensity. Even closer to the critical line longer delays might be required due to the divergence in critical slowing down.[37]

DLS for PS/CH Solutions (0.1 < *P*/MPa < 125), (293 < *T*/K < 341). (1) Pressure-Induced Slow Modes in CH (and MCH) Solutions. Data on the pressure dependence of DLS for PS/CH solutions are reported in Figure 2 and in Table 1 of the Supporting Information. At low pressure (90° scattering angle, near-critical concentration, 0.1 MPa) the predominant contribution to DLS is from Γ^{f}. As pressure increases with $T/T_{\Theta} > 1$, however, significant changes occur in the DLS patterns. To begin, and most prominently, slow modes make their appearance, showing ever increasing relative intensity as P grows isothermally, or (at constant P) as T drops toward T_{Θ}. Parts a and b of Figure 2 illustrate this effect by comparing CONTIN-deduced DLS intensity patterns for PS90K/CH solutions of near-critical concentration (12.98 wt %, $c/c^* = 0.65$, $c^* = 3M_w/(4\pi N_{av} r_g^3)$, where N_{av} is Avogadro's number and r_g the radius of gyration) at two pressures (90°, 0.5 MPa, 40 °C [$T - T_{\Theta} = 6.5$ K]) and (90°, 50MPa, 40 °C). Figure 2c plots the unfiltered and unsmoothed data from which the autocorrelation functions and subsequently parts a and b of Figure 2 were determined. The pressure-enhanced contribution of the slow mode is apparent in either the autocorrelation (Figure 2c) or CONTIN (Figure 2a,b) representations. It is significantly more than that observed at higher temperature or lower MW (PS30K/CH). Patterns are not shown for PS30K/CH because the slow-mode contribution for this solution is vanishingly small at any temperature. For M_w significantly larger than ~90K slow-modes are already prominent at $P = 0.1$ in solutions of near-critical concentration. At temperatures below T_{Θ} the overall DLS intensity markedly increases as the fast mode intensity rises toward its critical divergence, and the slow-mode relative contribution is damped. An increase in pressure typically serves to sharpen the fast peak and gradually move it toward higher values. An example is shown in parts d and e of Figure 2 [PS-90K/CH at near-critical concentration 12.98 wt % and two pressures (90°, 0.5MPa, 21.2 °C [$T - T_{\Theta} = -12.3$ K] and 90°, 24.6MPa, 21.2 °C)]. Figure 2f compares these results in CH solutions with DLS patterns for PS90K/MCHh at 85 °C (13 wt %; $c/c^* = 0.64$ where $c^* = 3M_w/(4\pi N_{av} r_g^3)$, N_{av} is Avogadro's number and, r_g the polymer radius of gyration). Under these conditions the relative intensities of the slow and fast contributions rises from $I^s/I^f \sim 1/7$ at 10MPa to $I^s/I^f \sim 4/1$ at $P >$ ~150 MPa. Methylcyclohexane is an appreciably worse solvent than is cyclohexane (so far as solvent quality correlates with UCST demixing loci), and presumably poorer solvent quality is why slow-mode pressure sensitivity in MCH persists to higher temperature. Even so, at the pressures and temperatures of the present studies, which show $(\partial I^s/\partial P) > 0$ for both CH and MCH solutions, the phase equilibrium studies reveal $(\partial(\text{USCT})/\partial P) > 0$ for CH and $(\partial(\text{UCST})/\partial P) < 0$ for MCH, respectively (compare slopes for LL equilibria in Figures 3a and 5a). One must conclude, therefore, that UCST solvent quality and slow-mode relative intensity are not correlated in any simple fashion. One might speculate that the pressure dependence of slow-mode intensity is consequent to pressure modulation of the viscosity and thence viscoelasticity, but such a conclusion is unwarranted, at least until slow-mode q dependence becomes established. In interpreting Figure 2, remember that scattering intensity is sensitive to particle size, and in no sense can plots of uncalibrated relative contributions of fast and slow

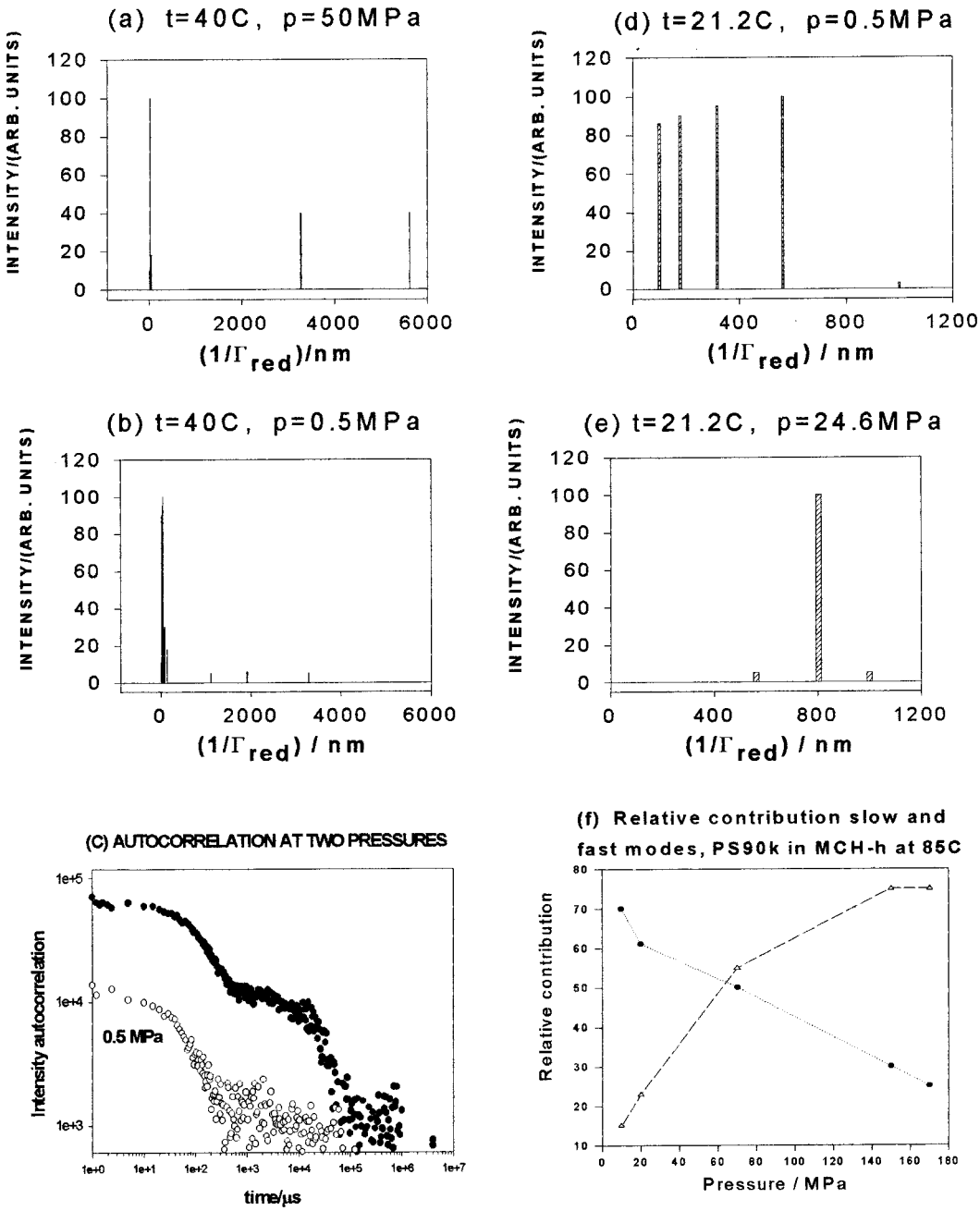

Figure 2. CONTIN patterns deduced from DLS correlation functions at various temperatures and pressures. Intensity is plotted vs reduced reciprocal relaxation time, $(1/\Gamma_{red}) = (kTq^2/(6\pi\eta\Gamma))$ which for the diffusive (fast) mode defines the correlation radius, ξ^f. For these experiments, $q = 0.014$ nm^{-1} and η is obtained from Table 2. (a and b) CONTIN patterns for PS90K/CH at near-critical concentration (12.98 wt %) at 0.5 and 50 MPa, 40 °C, $T - T_\Theta = 6.5$ K. The pressure enhancement of the slow-mode intensity is apparent. (c) The unfiltered and unsmoothed data determining the autocorrelation functions from which Figures 2a and 2b were determined. (d and e) CONTIN patterns for PS90K/CH at near-critical concentration (12.98 wt %) at 0.5 and 24.6 MPa, 21.2 °C. Under these conditions (near LL demixing), the slow-mode contribution is overwhelmed by the diverging fast mode contribution which sharpens with increasing pressure shifting to higher values and finally diverging as the critical point is approached. (f) Relative intensity contributions of fast- (solid circles) and slow-mode contributions (open triangles) to CONTIN patterns for PS90K/MCHh solutions at 85 °C as a function of pressure.

modes to CONTIN patterns be interpreted in terms of relative amounts of the species from which they arise.

(2) The Approach to Critical Demixing in PS/CH Solutions. In addition to *P*-induced appearance of Γ^s, DLS patterns for PS/CH and PS/MCH solutions show other marked changes as (T,P) conditions approach the LL equilibrium line (i.e. move to the poor solution side of T_Θ and or P_Θ). At LL it is well established that ξ^f and I^f diverge logarithmically, dominating and thus damping out (obscuring) the relatively small contributions of the slow mode. This is unfortunate, as information on slow-mode contributions near the LL transition would be of considerable interest. Near the LL transition we follow others[7,8,11,27] in assigning the fast contribution in the DLS pattern to diffusional intermolecular correlation. Speaking loosely, the claim is that the effect of a change in *P* or *T* in moving one closer to, or further from, LL amounts to nothing more than a change in solvent quality. Thus, the interpretation of ξ^f and I^f is tightly coupled to the location on the phase diagram.

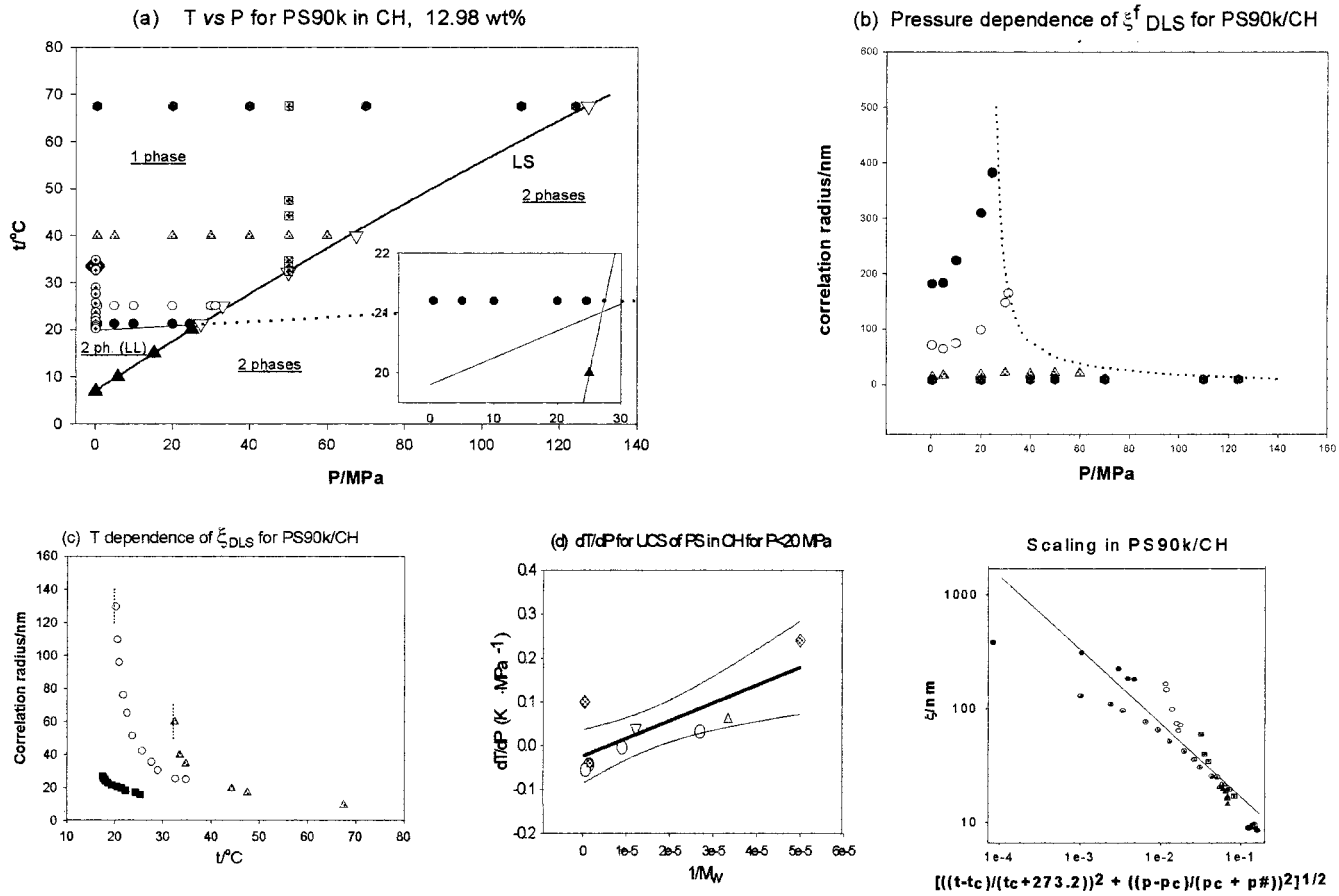

Figure 3. DLS of PS/cyclohexane solutions. (a) Location of the PS90K/CH 12.98 wt %, $c/c^* = 0.65$, DLS data net on the phase diagram. Solid circles = DLS 21.2 °C, open circles = DLS 25 °C, shaded triangles = DLS 40 °C, solid hexagons = DLS 67.5 °C, centered open circles = DLS 0.1 MPa isobar, shaded crossed squares = DLS 50 MPa, open inverted triangles = LS transitions determined by DLS (present work), and solid heavy triangles = low pressure LS transitions.[38] The heavy solid line is fit to low-pressure LS transitions and extrapolated.[38] $(P_{LS}(\mathrm{CH})/\mathrm{MPa}) = -12.4623 + 1.79268t/°\mathrm{C} + 4.042 \times 10^{-3}(t/°\mathrm{C})^2$. The lighter line (solid, then dotted, as P increases) shows the LL equilibrium line from Figure 3d [$t_{LL}(\mathrm{PS90K/CH}) = 19.8 + 0.045(P/\mathrm{MPa})$]. The diamond locates T_Θ (0.1 MPa). The insert magnifies the region close to the intersection of the LL and LS transition loci. (b) $[(1/\Gamma_{90}^f)_{red} \sim \xi^f]$ vs P for PS90K/CH, 12.98 wt % along isotherms (reading up) at 67.5 (hexagons), 40 (triangles), 25 (open circles) and 21.2 °C (solid circles). (c) $[(1/\Gamma_{90}^f)_{red} \sim \xi^f]$vs T for PS90K/CH, 12.98 wt % along isobars at 50 (triangles) and 0.1 MPa (open circles), and for 3.25 wt % at 0.1 MPa (squares). The dotted lines locate transition temperatures which for 50 MPa are LS and for 0.1 MPa are LL, respectively. (d) dT_{LL}/dP for demixing of polystyrene/cyclohexane solutions. Circle = ref 39, upside down triangle = ref 40, square = ref 41, triangle = ref 42, and diamond = ref 43. The correlation line is $(dT_{LL}/dP)/(\mathrm{K{\cdot}MPa^{-1}}) = -0.025 + 4055/M_w$. (e) Reduced scaling representation of the data in parts b and c. The correlation line is $\log(\xi^f/\mathrm{nm}) = 0.58 - 0.65 \log R_{red}$ ($r^2 = 0.85$, $p^\# = 5500$, $t^\# = 273.2$). The uncertainty in the scaling exponent (limiting slope) is ~0.06, $d\nu/\nu \sim 0.1$. Symbols are the same as in part a.

Figure 3a locates the DLS data-net (PS90K/CH, 13.0 wt %, $c/c^* = 0.64$) on the phase diagram. The data sample the region near the LL and LS demixing lines (the latter is presumably precipitation of solid cyclohexane[38]). They include isobars at 0.1 and 50 MPa extending from 67.5 °C ($T - T_{\Theta,0.1\mathrm{MPa}} = 34.0$) to the LL or LS transitions at 19.8 °C ($T - T_{\Theta,0.1\mathrm{MPa}} = -13.7$) and 32.1 °C ($T - T_{\Theta,0.1\mathrm{MPa}} = -1.4$) respectively, and isotherms at 67.5, 40, 25, and 21.2 °C ($[T - T_{\Theta,0.1\mathrm{MPa}}] = 34.0, 6.5, -8.5$, and -12.3). Parts b and c of Figure 3 show the P and T dependences of ξ^f (I^f, not shown in the figures, behaves analogously). For $T/T_\Theta < 1$ both ξ^f and I^f diverge as T falls (Figure 3c) or P rises (Figure 3b), toward T_{LL} and P_{LL}, respectively.

(3) Discussion. To interpret the data we follow Szydlowski and Van Hook[7,8] and review changes expected in DLS correlograms at ambient pressure as one moves from the homogeneous part of the phase diagram (i.e., well to the good solvent side of T_Θ) inducing precipitation by temperature quench. In the homogeneous region well-defined monomodal single-exponential correlograms are observed at low to moderate MW, but at higher MW the situation is complicated by the appearance of the slow transient gellike network modes discussed earlier,[11] (although most of the present experiments in CH are for PS-90000, where the MW is too small to show these modes at 0.1 MPa). At concentrations below overlap ($c(\mathrm{overlap}) = c^* = 3M_w/(4\pi N_{av} r_g^3)$, N_{av} is Avogadro's number and r_g the radius of gyration), ξ^f decreases, but slowly, as temperature falls below the LL coexistence line and into the metastable region. That pattern ends at the cloud point where the correlogram splits abruptly and discontinuously yielding a bimodal distribution, the splitting process is sensitive to both quench depth and quench rate, and precipitation follows the nucleation-growth mechanism (NG). At higher concentration LL demixing is via the spinodal decomposition-percolation (SD/P) mechanism. In this region one finds well behaved monomodal DLS correlograms which show exponentially increasing ξ^f and I^f as the cloud point is approached, and at critical concentration both diverge.

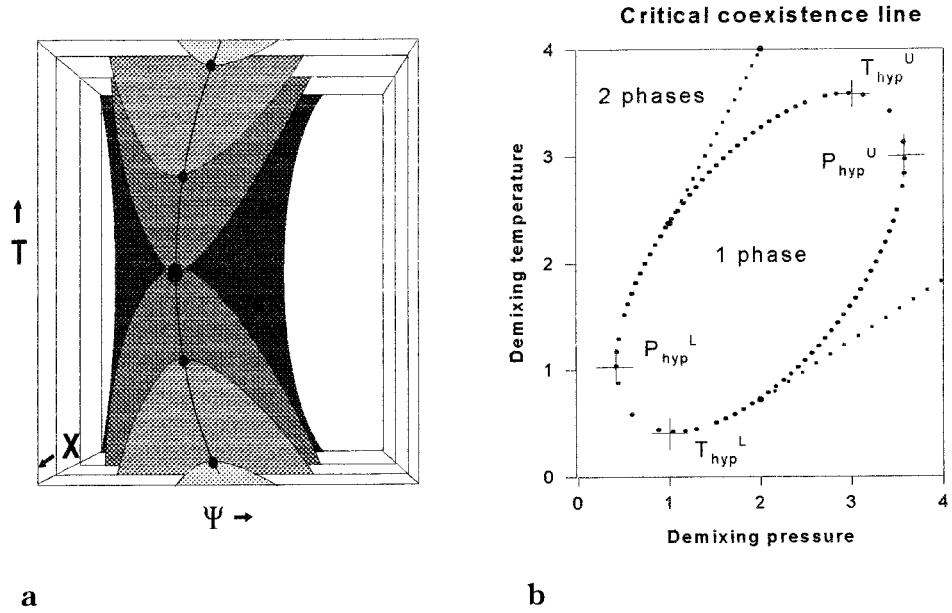

Figure 4. (a) LL demixing of solutions of the PS/MCH type (schematic). The upper and lower two-phase regions are shaded. The X coordinate may be MW ($X = MW^{-1/2}$) at constant pressure, pressure at constant MW, or another variable of interest. The upper and lower branches join at the hypercritical point (large dot) which may occur at either positive or negative X. (b, right) Example of a closed (or open, lightly dotted) coexistence line in the $(T,P)_{\psi(cr)}$ projection (schematic).

The present data are complicated by the fact they extend to pressures high enough to induce the LS solvent transition. At the freezing point both scattered and transmitted intensities discontinuously drop, ending the experiment. The $(P,T)_{freezing}$ loci thus determined are shown as the inverted open triangles in Figure 3a. The solid upright triangles in the figure show the freezing points for pure CH reported by Matsuo and Van Hook,[38] and the heavy correlation line drawn through the triangles and extrapolated to 130 MPa is a least-squares fit of those low-pressure data. The excellent agreement between the solution freezing points and the extrapolated correlation line for the pure solvent LS transition confirms the assignment. (In this connection it is useful to estimate the freezing point depression for the polymer solution. We find $\Delta T \sim [RT^2/\Delta H^o_{fus}(CH)]x_{PS} \sim 0.04$ K using the 0.1 MPa tabulated value of $\Delta H^o_{fus}(CH)$ and approximating the solution as ideal. It is unlikely that solution nonideality will cause the estimate to err by as much as 0.01 K. The correction for freezing point depression is thus negligible on the scale of Figure 3a.)

The present data are at large enough concentration to ensure that LL precipitation, when it occurs, follows SD/P. At 0.1 MPa and 90000 MW the correlogram is monomodal. For this solution both ξ^f and I^f increase as T falls or pressure increases. In either case the change moves one closer to the LL equilibrium line. The pressure effect is mildly unusual; most PS/solvent systems we have studied[1-10] show an improvement in solvent quality as P increases. Along UCS that implies $dT_{LL}/dP < 0$. The PS/CH LL transition under discussion is of the UCS class, but the available data show $dT_{LL}/dP \sim 0$, varying from slightly positive at low MW to slightly negative at higher MW. Those data[39-43] are plotted in Figure 3d which establishes $(dT_{LL}/dP)_{PS90K} > 0$, in agreement with the prediction from the DLS patterns (Figure 3b,c), although the data scatter appreciably. The LL equilibrium line in Figure 3a was plotted by taking $(dT_{LL}/dP)_{CH90K}$ consistent with Figure 3d (and independent of pressure) and using T_{LL}(0.1 MPa) = 19.2 °C. The insert to Figure 3a rationalizes the pressure dependence of ξ^f and I^f along the 21.2 °C isotherm which, with increasing pressure, steadily approaches the LL equilibrium line, but at an acute angle. It has almost, but not quite, reached the LL transition line by the time it intersects LS whereupon solvent crystallization intervenes, ending the experiment.

Figure 3e shows the entire PS90K/CH data net plotted in the reduced scaling representation developed below. A significant improvement in efficiency of representation is apparent in comparing Figure 3b or Figure 3c with Figure 3e. The LL demixing curve lies nearly flat in the (T,P) plane and this accounts for a very large and poorly defined value for the scaling parameter, $p^{\#}$, and the associated uncertainty in the scaling exponent (reported in the caption). It is likely that uncertainties in the curvature of the LL equilibrium line (Figure 3d), which is not experimentally well defined, account for the bulk of the scatter, isotherm to isotherm, or isobar to isobar. These uncertainties confirm that the PS/MCH data presented below are better suited for the investigation of reduced scaling in the $(T,P)_{\psi cr}$ plane.

DLS Correlation Radii in the (P, T, ψ_c) Projection for PS/MCH. (1) A Reentrant Phase Diagram. Figure 4 is a schematic LL demixing diagram for polymer/solvent systems with both UCS and LCS branches. Two-phase (shaded) regions lie at the top and bottom centers. Temperature, T, is plotted against concentration of polymer, ψ, in the plane of the paper. The third variable extending into the page might be molecular weight, pressure, or some other variable of interest. For the moment we select pressure as the third variable, holding MW at a convenient value to ensure that the upper and lower branches join at an accessible pressure. The heavy line connecting critical points on the UCS and LCS branches and running through the double critical point (hypercritical point) is plotted in the $(T,P)_{\psi(cr)}$ projection in Figure 4b. Although curvature of the demixing locus in this projection is not thermo-

dynamically required, our interest is in systems (such as PS/MCH) where appreciable curvature is found. The two possibilities sketched in the insert show sufficient curvature to display extrema at lower T and P, but one is open and the other closed at higher T and P. For the moment, we turn attention to the latter possibility, labeling the four extrema as upper and lower hypercritical temperatures, $T_{hyp}{}^{U}$ and $T_{hyp}{}^{L}$, and upper and lower hypercritical pressures, $P_{hyp}{}^{U}$ and $P_{hyp}{}^{L}$, respectively.

PS/MCH solutions form examples of at least the lower part of the reentrant diagram illustrated in Figure 4. Previous observations of the demixing diagram for PS/MCH at modestly elevated pressures have been reported by Vanhee et al.[44] ($0.1 < P/\text{MPa} < 90$), Van Hook et al.,[4,9,10] Enders and de Loos,[45] Hosokawa, Nakata, and Dobashi,[46] and Wells et al.[47] and correlated by Imre and Van Hook.[6] The earlier work establishes the existence of a lower hypercritical temperature ($T_{hyp}{}^{L} = 305$ K, 55 MPa, at $M_w(\text{PS}) = 3 \times 10^4$), and points to the existence of a lower hypercritical pressure at $P < 0$, but not too deep ($P_{hyp}{}^{L} = \sim 34\,010$ K, $\sim -15 \pm 3$ MPa at $M_w(\text{PS}) = 3 \times 10^4$, dropping off to $P_{hyp}{}^{L} = \sim 360 \pm 10$ K, $\sim -10 \pm 3$ MPa, at $M_w(\text{PS}) = 2 \times 10^6$). In the present study we were interested in determining ξ^f near the LL phase transition as a function of the direction of approach to demixing (especially in the region close to hypercritical points), and also in extending the (P,T) range of the measurements in an attempt to locate $P_{hyp}{}^{U}$ and $T_{hyp}{}^{U}$, should they exist.

Closed loop reentrant phase diagrams in the (T,ψ) plane have been discussed by Narayanan and Kumar,[48] and in (T,P,ψ) space by Schneider.[49] Many of the thermodynamic properties of this type of diagram are discussed or implied in the developments of Prigogine and Defay[50] and Rice.[51] From that type of analysis we conclude that any simple Flory−Huggins or modified Flory−Huggins model leading to a closed loop in the $(T,P)_{cr}$ projection must include T- and P-dependent excess free energy parameters (χ_g). A simple equation which predicts a closed loop and satisfies the thermodynamic constraints is found when the χ parameters describing the excess volume and the excess enthalpy are each dependent on T and P, but in compensatory fashion.

Experimental Results

Curvature in the $(T,P)_{\psi cr}$ Projection for PS/MCH Solutions. We report DLS investigations in the reentrant region of the PS/MCH phase diagram at several MWs and isotopic labels for ($0.1 < P/\text{MPa} < 200$) and ($32 < t/°\text{C} < 88$) in Table 2, Supporting Information (PS30K/MCHd, PS30K/MCHh, PS90K/MCHh, PS400K/MCHh). Our purpose in extending earlier work[4,9,10,39−41,44−47] was 2-fold: (1) A successful attempt to locate a complete set of hypercritical temperatures and pressures (closed loop), should they exist, would be of great benefit in constraining and thus accurately defining the mean field parameters in the equation of state which describes the solution.[3] Unfortunately the present results show that if the upper hypercritical points, $T_{hcp}{}^{U}$ and $P_{hcp}{}^{U}$, exist, they lie above the maximum T or P of the present experiments. Thus, the present study is limited to an examination of just the lower part of the reentrant diagram. (2) The well-defined location of a curved critical surface permits one to explore questions concerning the proper thermodynamic path to employ in multidimensional scaling descriptions of the approach to criticality. It is clear from the geometrical picture of phase transitions, originally due to Griffiths and Wheeler,[52] that direction of approach to criticality is essential in determining the value of the scaling exponents describing properties such as correlation length, susceptibility, compressibility, etc.[48] For T and P accessible to us, we were only able to locate $P_{hyp}{}^{L}$ and $T_{hyp}{}^{L}$. $P_{hyp}{}^{U}$ and $T_{hyp}{}^{U}$, if they exist, lie substantially above 200 MPa and 400 K, respectively.[53] Even so, the data reported in the Supporting Information and shown in Figures 5 and 6 are of interest. Most of these data are at critical or near-critical concentrations.[6] They include extensive data sets for PS30K dissolved $MCHh_{14}$ (11.5 wt %, 12.1 segment %, $c/c^* = 0.21$) and $MCHd_{14}$ (11.4 wt %, 13.3 segment %). Although referring to slightly different concentrations, the (T,ψ) curves are very flat in the region of the maximum, and both solutions are at near-critical concentrations. The data nets are shown in Figure 5a. We chose deuterated solvent to permit direct comparison with SANS data on identical solutions.[10,34] Deuterated solvent (or solute) is required in SANS in order to set the contrast. Unfortunately the SANS quartz window cell is rated to only 50 MPa so we were unable to explore the LL transition near $T_{hcp}{}^{L}$ with SANS. SANS/DLS comparisons in the range 0−50 MPa are discussed in a later section. The equations used to describe the shape of the LL equilibrium lines in the $(T,P)_{\psi cr}$ projections are reported in the caption. Parts b−d of Figure 5 show ξ^f, I^f, and D (diffusion constant) for PS30K/MCHd, and include comparisons with PS30K/MCHh. Divergences in ξ^f and I^f as the critical line is approached by increasing or decreasing P, or by decreasing T, are apparent. Most of the discussion which follows will focus on ξ^f but is easily rephrased in terms of D or Γ^f by invoking eq 1 and Table 2. The behavior of I^f is analogous to that of ξ^f (i.e. diverging as the critical locus is approached), but run-to-run comparisons are not so precise as for ξ^f because the experimental protocol involved neither absolute nor relative (run to run) calibrations of scattering intensity.

Parts a−d of Figure 6 show the DLS data net superposed on the LL phase diagram in the $(T,P)_{\psi cr}$ projection (Figure 6a), ξ^f vs T (Figure 6b) and P (Figure 6c), and D for PS90K/MCHh and PS400K/MCHh solutions (Figure 6d). MCHh is a better solvent than MCHd, and the increased MW (30K to 90K) moves the LL equilibrium line to a convenient location. LL equilibrium lines for PS30K/MCHd (11.4 wt %, 0.121 segment fraction, $c/c^* = 0.21$), PS90K/MCHh (12.98 wt %, 0.123 segment fraction, $c/c^* = 0.64$), and PS400K/ MCHh (8.9 wt %, 0.084 segment fraction, $c/c^* = 0.58$) are compared in Figure 6a. The behavior of ξ^f, I^f, and D as the LL critical locus is approached is qualitatively the same for PS90K/MCHh (Figure 6b−d) and PS400K/MCHh (not shown in entirety) as for PS30K/MCH (Figure 5).

A Scaling Representation of the DLS and SANS Correlation Radii. Narayanan and Kumar[48] comment, "...the most compelling issue concerning experimental investigations of reentrant phase transitions (RPT's) is how to recover universal exponents for the RPT. In other words which field variable should be used in place of ...?", and elsewhere, "In other words, it is difficult to obtain the correct thermodynamic path in the multidimensional field space". In common with others they demonstrate that a doubling of critical exponents follows from the geometrical model of RPT's for data sufficiently

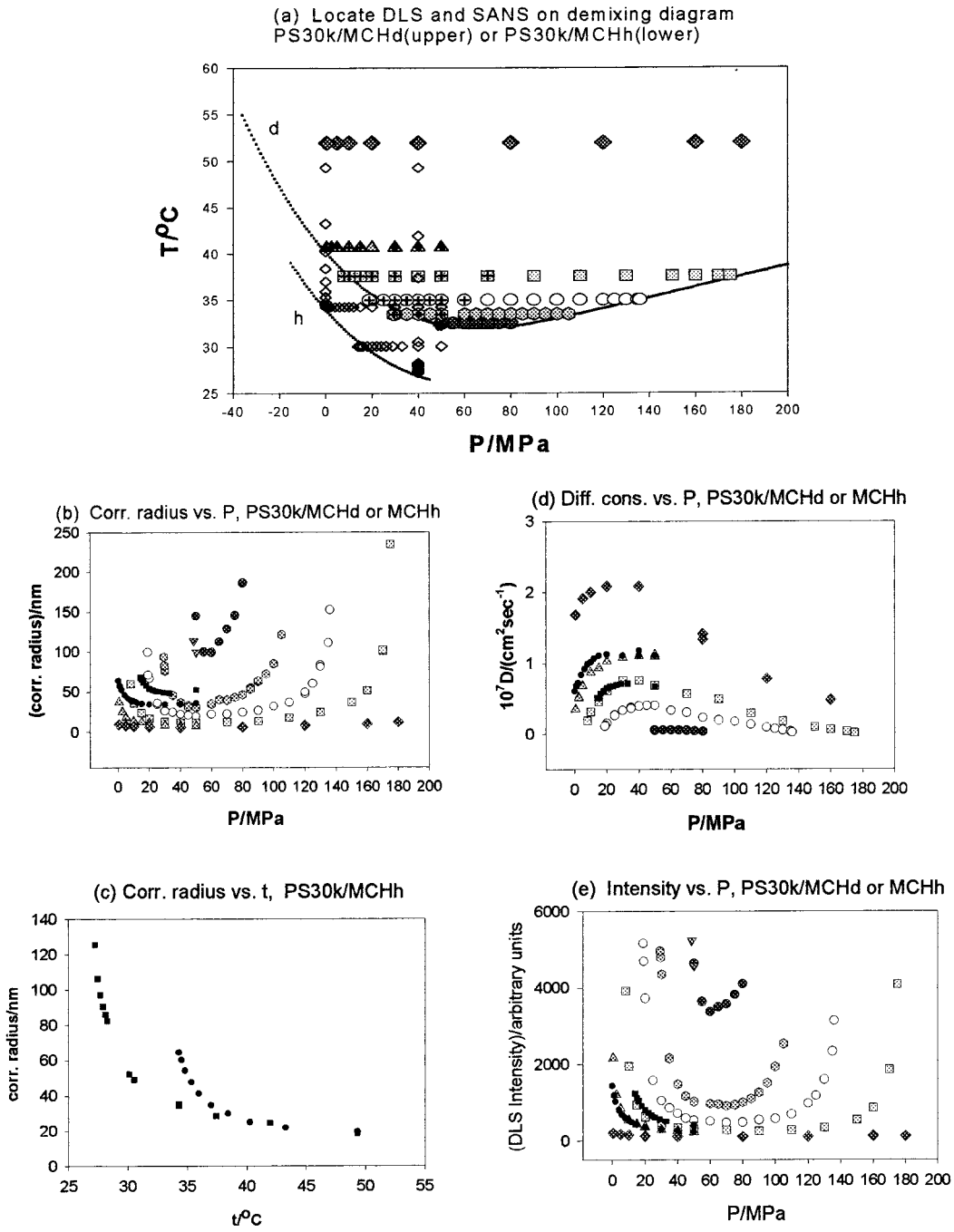

Figure 5. DLS of PS/methylcyclohexane solutions. (a) Location of the PS30K/MCHd, (11.4 wt %) $c/c^* = 0.21$, and PS30K/MCHh (11.5 wt %) DLS and SANS data nets on the phase diagrams. Demixing isopleths (upper = MCHd, lower = MCHh) were determined by visual observation or LS. The LL equilibrium lines are $t_{LL}(\text{PS30K/MCHd})/°C = 39.08 - 0.264(P/\text{MPa}) + 2.97 \times 10^{-3}(P/\text{MPa})^2 - 9.24 \times 10^{-6}(P/\text{MPa})^3$ for $-40 < P/\text{MPa} < 108$, $t_{LL}(\text{PS30K/MCHd})/°C = 33.63 + 0.058((P/\text{MPa}) - 108)$ for $200 > P/\text{MPa} > 108$, and $t_{LL}(\text{PS30K/MCHh})/°C = t_{LL}(\text{PS30K/MCHd})/°C - 6.2$, all limited to $P/\text{MPa} < 200$. Shaded circles = DLS 32.5 °C, shaded inverted triangles = DLS 32.3 °C, lightly shaded hexagons = DLS 33.5 °C, open circles = DLS 35 °C, lightly shaded squares = DLS 37.6 °C, lightly shaded triangles = DLS 40.7 °C, and shaded diamonds = DLS 52.3 °C, all for MCHd solutions. The heavy crosses locate SANS in MCHd, and the small open diamonds, DLS in MCHh solutions. (b) $[(1/\Gamma^f_{90})_{red} \sim \xi^f]$ vs P for PS30K/MCHd and MCHh solutions. The symbols for MCHd are the same as in part a. In MCHh the small solid circles and small solid squares locate data at 34.3 and 30.1 °C, respectively. In the region of the hypercritical minimum, $T_{hyp}{}^L$, ξ^f diverges, as expected, as P increases or decreases approaching the critical locus. (c) $[(1/\Gamma_{90}{}^f)_{red} \sim \xi^f]$ vs T for two isobars in PS30K/MCHh. The small solid circles and small solid squares locate data at 0 and 40 MPa, respectively. ξ^f diverges, as expected, on the approach to the critical locus. (d) DLS diffusion constants vs P for PS30K/MCHd and MCHh solutions. The symbols are the same as in parts a and b. For the isotherm at $T_{hyp}{}^L$ D falls to zero as P increases or decreases and approaches the critical locus. (e) DLS intensity vs P for PS30K/MCHd and MCHh solutions. The symbols are the same as in Figure 5a. In the region of $T_{hyp}{}^L$, I^f diverges as P increases or decreases and approaches the critical locus.

close to the critical line (provided that line be quadratic in the vicinity of the hypercritical turning point). Near $P_{hcp}{}^L$ or $P_{hcp}{}^U$, it is a properly defined reduced temperature which should demonstrate the doubling; near $T_{hcp}{}^L$ or $T_{hcp}{}^U$, it is a properly reduced pressure. The authors remind us that the properly defined thermodynamic scaling variable can nowhere be tangent to the critical curve. They go on to cite recent examples from their own

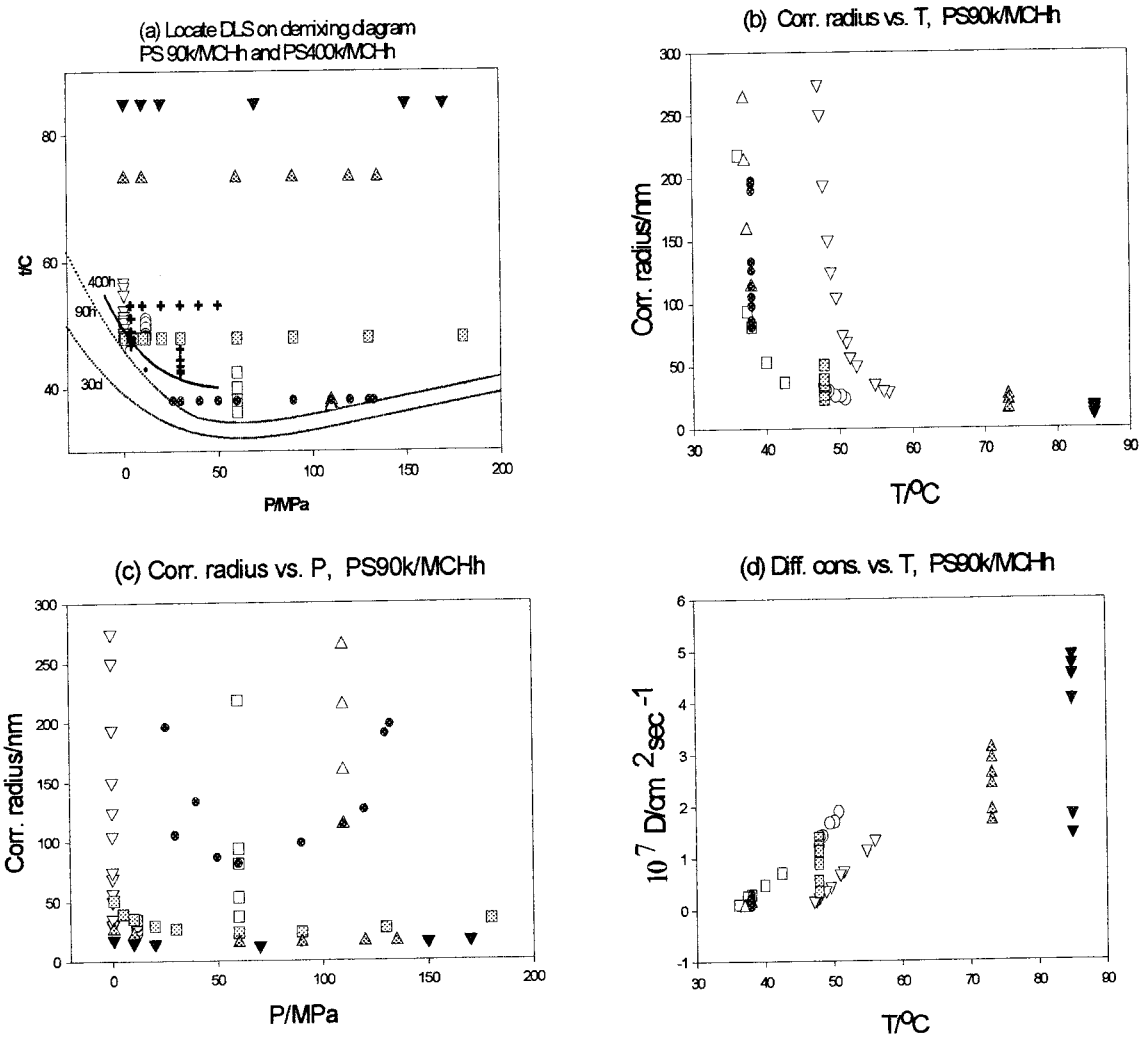

Figure 6. (a) Location of the PS90K/MCHh (12.98 wt %), $c/c^* = 64$, and PS400K/MCHh (8.9 wt %, $c/c^* = 0.58$) DLS data nets on the phase diagrams. Demixing isopleths determined by visual observation or LS (lines) are t_{LL}(PS90K/MCHh)/°$C = t_{LL}$(PS30K/MCHd) + 7.0 − 0.15 (P/MPa) + 5 × 10^{-4} (P/MPa)^2 + 10^{-5} (P/MPa)^3 for ∼−30 < P/MPa < 40, t_{LL}(PS90K/MCHh)/°$C = t_{LL}$(PS30K/MCHd) + 2.5 for 40 < P/MPa < 200, and t_{LL}(PS400K/MCHh)/°C = 49.3 − 0.46 (P/MPa) + 8.1 × 10^{-3} (P/MPa)^2 + 10^{-4} (P/MPa)^3 for −10 < P/MPa < 50 (upper line). The lowermost line is LL for PS30K/MCHd from Figure 5a. For PS90K/MCHh open points are isobars, and solid and shaded points are isotherms. Shaded circles = 38.0 °C, lightly shaded squares = 47.9 °C, lightly shaded triangles = 73.2 °C, shaded inverted triangles = 85.0 °C, open inverted triangles = 0.1 MPa, open circles = 11.6 MPa, open squares = 60 MPa, and open triangles = 110 MPa. Heavy crosses locate DLS data points for PS400K/MCHh (8.9 wt %). (b) $[(1/\Gamma_{90}^{f})_{red} \sim \xi_{DLS}^{f}]$ vs T for PS90K/MCHh, with symbols the same as part a. The divergence as T falls to the critical locus is apparent. (c) $[(1/\Gamma_{90}^{f})_{red} \sim \xi^{f}]$ vs P for PS90K/MCHh, with symbols the same as part a. Near $T_{hyp}{}^{L}$, $\xi_{DLS}{}^{f}$ diverges as P increases or decreases and approaches the critical locus. (d) DLS diffusion constants vs T for PS90K/MCHh, with symbols the same as part a. The drop-off to $D = 0$ as T or P approaches the critical locus is apparent.

work[48,54,55] and the literature[48] supporting the analysis. Hosakawa, Nakata, and Dobashi[46] take a similar approach in their analysis of the coexistence surface for PS/MCHh (MW = 10K, 16K, and 35K, 0 < P/MPa < 80) solutions. In that study, closely related to the one described in this paper, they find $\beta_d = 2\beta_o$ in good agreement with $\beta_{o,theory} = 0.325$ for isotherms very close to $P_{hcp}{}^{L}$ (the critical double point, CDP, in their notation); β_o is the scaling exponent which describes the shape of the coexistence curve in the vicinity of the critical point.

The present data extend over a wide range and in no sense carefully sample the region in the immediate vicinity of the hypercritical points. Furthermore, over the range of these experiments, the critical line is markedly asymmetric for an expansion about $P_{hcp}{}^{L}$. We require a different approach and have developed an empirical two-dimensional scaling formalism to describe scattering data in the $(T,P)_{\psi cr}$ plane. Mindful of the admonition that at no point should the relevant field variable be tangent to the critical line we have elected to develop scaling in terms of a variable, R_{red}, defined as the minimum distance (hence the perpendicular) from the experimental point of interest to the LL critical line in an appropriately reduced space.

$$R_{red} = \{[(t_{exp} - t_{cr})_{min}/(t_{exp} + t^{\#})]^2 + [(p_{exp} - p_{cr})_{min}/(p_{exp} + p^{\#})]^2\}^{1/2} \quad (2)$$

In eq 2, (t_{exp},p_{exp}) and $(t_{cr},p_{cr})_{min}$ are the coordinates of the experimental point of interest and that point on the critical line which is a minimum distance from the experimental point, respectively, and $t^{\#}$ and $p^{\#}$ are reduction parameters.

Further discussion is appropriate. Should the field variable lie parallel to t, an appropriate scaling equation

Table 3. Least-Squares Regression Parameters for Scaling Fits to Eq 9

solution	argument[a]	$(c/c^*)^b$	A	$-\nu(\mathrm{d}\nu)^c$	r^2	$p^\#$
PS0K/MCHh	$\xi - R_h$	0.21	0.58	0.57 (0.06)	0.98	55
PS30K/MCHd	$\xi - R_h$		0.35	0.72 (0.07)	0.91	55
	$\xi_{SANS} - R_g$		−1.02	0.75 (0.1)	0.84	55
PS90K/MCHh	$\xi - R_h$	0.64	0.51	0.74 (0.07)	0.90	55
PS400K/MCHh	$\xi - R_h$	0.58	0.80	0.55 (0.1)	0.76	55
all MCH data	$\xi - R_h$		0.44	0.68 (0.05)	0.89	55
together	(intensity)		0.87	0.83 (- -)	0.65	55
PS90K/CHh	ξ	0.65	0.58	0.65 (0.07)	0.85	5500

[a] R_h (hydrodynamic radius) taken as 3, 6, and 11 nm for PS30K, -90K, and -400K, in MCH. R_g (radius gyration) for PS30K in MCHd taken as 4 nm, both to nearest integer.[58] Nonsubscripted ξ values refer to data obtained by dynamic light scattering, subscripted to data from small-angle neutron scattering. [b] Here $c^* = 3M_w/(4\pi N_{av} r_g^3)$, N_{av} is Avogadro's number, and r_g is the polymer radius of gyration. [c] Uncertainty in scaling exponent estimated from plots at 99% confidence interval.

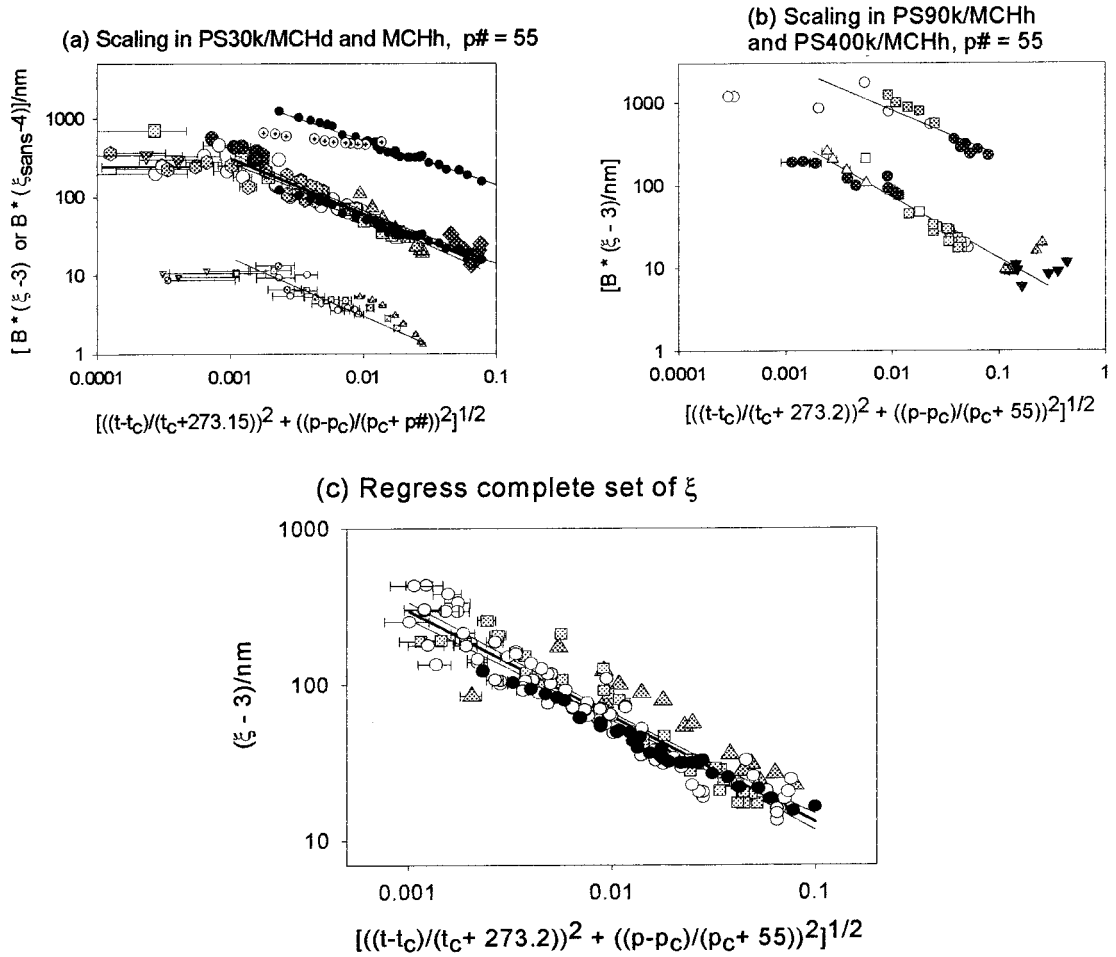

Figure 7. Reduced scaling of DLS and SANS data for PS/MCH solutions, $p^\# = 55$, $t^\# = 273.2$. (a) PS30K/MCHd and PS30K/MCHh. The top curve is DLS in MCHh setting $B = 10$ to avoid overlap of the plot with that for PS30K/MCHd (middle line, $B = 1$). For the upper line (PS30K/MCHh, $B = 10$), the open circles denote the 30.1 °C isotherm; these points are not included in least squares analysis, the solid circles show the rest of the data for PS30K/MCHh. The middle line shows DLS data for PS30K/MCHd ($B = 1$, symbols defined in caption of Figure 5) and PS30K/MCHh ($B = 1$, solid circles). DLS data in MCHh and MCHd lie atop one another within experimental error. The lower curve ($B = 1$) is the fit to the SANS data.[10] Least squares parameters for the regression lines are reported in Table 3. (b) Scaling for PS90K/MCHh (12.98 wt %) DLS, (lower line, $B = 1$) symbols defined in caption of Figure 6 and PS400K/MCHh (8.9 wt %) DLS, (upper line, $B = 10$). Symbols for the upper line are defined in caption of Figure 6. Least-squares parameters are reported in Table 3. (c) Combined scaling fit of all DLS data ($0.001 < R_{red} < 0.1$): shaded triangles = PS400K/MCHh (8.9 wt %), shaded squares = PS90K/MCHh (12.98 wt %), open circles = PS30K/MCHd (11.4 wt %), and solid circles = PS30K/MCHh (11.5 wt %). Least-squares parameters reported in Table 3.

for the correlation radius might be $\xi_t = A_t[|(t_{exp} - t_{cr})/(t_{cr} + t^\#)|]^\nu = A_t\tau^\nu$ where τ is a reduced temperature and n a scaling exponent. By including the constant $t^\#$, difficulties are avoided, most obviously for the case when $t_{cr} \sim 0$. Along the temperature coordinate, that issue is often avoided by choosing t (°C) and setting $t^\# = 273.2$, i.e. assuming that it is T/K which properly scales temperature. In the pressure domain we write, similarly (should the field variable lie parallel to p), $\xi_p = A_p[|(p_{exp} - p_{cr})/(p_{cr} + p^\#)|]^\nu = A_\pi\pi^\nu$. Luszczyk, Rebelo, and Van Hook[2] have discussed the rationale for setting $t^\# = 273.2$ °C and have suggested a method to estimate $p^\#$, but for the moment we choose to regard $p^\#$ as an adjustable parameter and define the compound scaling as

$$\xi_R = A_R\{[\tau^2 + \pi^2]^{1/2}\}^\nu = A_t R_{red}{}^\nu \qquad (3)$$

i.e. choosing a coordinate set which is orthogonalized

by the transformation. A proper selection of the constants $t^{\#}$ and $p^{\#}$ ensures commensurate treatment of the t and p field variables. Similarly, expanding the argument, in (t, p, z) space, where z is an additional intensive variable, one could write $R_{red} = (\tau^2 + \pi^2 + \zeta^2)$, where $\zeta = [(z - z_{cr})/(z_{cr} + z^{\#})]$.

The Scaling Fits. R_{red} was calculated using expressions for the LL equilibrium lines reported in the captions of Figures 5 and 6, setting $t^{\#} = 273.2$ °C as is customary, and selecting $p^{\#}$ (MCH) = 55 MPa by smoothing the PS30K/MCHd data set. The calculation is not sensitive to the choice of $p^{\#}$, and we have elected to employ a universal value of $p^{\#}$ for all MCH solutions. Scaling fits are shown in Figure 7a−c. Least-squares regression lines for fits to eq 3 are reported in Table 3 together with the estimated uncertainty in the scaling exponent, n, obtained from fits to the plots at the 95% confidence interval.

$$\log (\xi^f - r_h) = A + \nu \log R_{red} \quad \text{or}$$

$$\log(\xi_{SANS} - r_g) = A + \nu \log R_{red} \quad (4a)$$

$$\log I(\xi^f) = A + \nu \log R_{red} \quad (4b)$$

In eq 4 we have used the fact that the static and dynamic correlation lengths far from the transition approach r_g and r_h, respectively. The error bars shown in Figure 7 document our best estimate of the uncertainty in R_{red}, $dR_{red} \sim 2.5 \times 10^{-4}$ and 7.5×10^{-4} for DLS and SANS, respectively. In each case the regressions are limited to $R_{red} > 10^{-3}$ avoiding the region of largest uncertainty. The dispersion in the scaling fits to ξ^f is likely accounted for by uncertainties in the definition of the critical line $(T,P)_{cr}$, coupled with uncertainties in the ratio $p^{\#}/t^{\#}$. The dispersion in the fits to I^f is significantly larger. It reflects run-to-run experimental error arising from the failure to compare scattered intensities to a standard. Each run involves removal and replacement of the scattering cell and consequent changes in transmitted and scattered intensity. The apparent fall off in scaling exponent, ν, for $R_{red} < 10^{-3}$ (see Figure 7a, for example) is likely an artifact. To begin, it is only observed where the relative uncertainty dR_{red}/R_{red} is increasing rapidly, i.e. for very small R_{red} at (T,P) very near the LL critical line. Imre and Van Hook[56] have shown that the effect is expected should the concentration be slightly off-critical.

The scaling exponents reported in Table 3 for both DLS and SANS are within experimental error of the theoretical value, $\nu = 0.63$.[48,57] It is remarkable that data in both H- and D-substituted solvents which extend over more than a decade in MW and more than two decades in R_{red} lie on a common scaling line. We felt that this important result strongly confirms the usefulness of the present approach for the fitting of scattering data in reentrant systems at T and P far from hypercritical points (critical double points). We think it particularly interesting that the ratio of DLS and SANS correlation radii remains nearly constant ($\xi_{DLS}/\xi_{SANS} \sim 14$) over a more than 50-fold change in R_{red}, even though the ratio of wavelengths of the probe radiations is more than 10^3 ($\lambda_{DLS}/\lambda_{SANS} = 1332$). Thus, it seems likely that the two techniques are measuring closely related structural correlations, albeit that one is static and the other dynamic in nature.

Conclusions

In this paper we have reported on a new apparatus to measure DLS (90°) of polymer solvent mixtures and have employed it in investigations on PS/cyclohexane and PS/methylcyclohexane solutions in the neighborhood of their LL transitions. Three important observations have resulted. (1) In both solutions, we detected pressure-enhanced slow modes. The pressure and temperature dependences of ξ^f and ξ^s and their relative contributions to the DLS scattering intensities are reviewed in Figure 2. While it is tempting to assign the new modes induced by the pressure dependence of the solution viscosity (which is marked) to transient viscoelastic network modes of the type discussed by Brown and others,[11,12] that is not possible in the absence of information on the q dependence of these modes. Further experiments are indicated. (2) DLS correlation radii extending over broad ranges of P, T, and MW ($0 < P$/MPa < 200), ($19 < t$/°C < 85), ($3 \times 10^4 <$ MW/amu $< 4 \times 10^5$) for the reentrant PS/MCH system have been fit within acceptable precision using a two-dimensional reduced scaling formalism in the (T,P) plane. The scaling exponent derived from the data is in good agreement with the theoretically expected value. (3) For PS/CH systems the correlation of the scattering and the phase equilibrium data for PS/CH is complicated by the pressure dependence of CH freezing but over the limited range available for study, the data can be represented using reduced scaling.

Acknowledgment. This work was supported by the U. S. Department of Energy, Division of Materials Sciences (DE88ER45374).

Supporting Information Available: Tables of DLS data for polymer mixtures. This material is available free of charge via the Internet at http://pubs.acs.org.

References and Notes

(1) Szydlowski, J.; Van Hook, W. A. *Macromolecules* **1991**, *24*, 4883.
(2) Luszczyk, M.; Rebelo, L. P. N.; Van Hook, W. A. *Macromolecules* **1995**, *28*, 745.
(3) Luszczyk, M.; Van Hook, W. A. *Macromolecules* **1996**, *29*, 6612.
(4) Imre, A.; Van Hook, W. A. *J. Polym. Sci., Polym. Phys.* **1996**, *34B*, 751.
(5) Imre, A.; Van Hook, W. A. *J. Polym. Sci., Polym. Phys.* **1994**, *32B*, 2283.
(6) Imre, A.; Van Hook, W. A. *J. Phys. Chem. Ref. Data* **1996**, *25*, 637.
(7) Szydlowski, J.; Van Hook, W. A. *Macromolecules* **1998**, *31*, 3255.
(8) Szydlowski, J.; Van Hook, W. A. *Macromolecules* **1998**, *31*, 3266.
(9) Szydlowski, J.; Rebelo, L. P. N.; Wilczura, H.; Van Hook, W. A.; Melnichenko, Y.; Wignall, G. D. *Fluid Phase Equilib.* **1998**, *150/151*, 687.
(10) Szydlowski, J.; Rebelo, L. P. N.; Wilczura, H.; Dadmun, M.; Melnichenko, Y.; Wignall, G. D.; Van Hook, W. A. *Physica B* **1998**, *241−243*, 1035.
(11) Brown, W.; Nicolai, T. In *Dynamic Light Scattering. The method and some applications*; Brown, W., Ed.; Clarendon Press: Oxford, England, 1993; Chapter 6, pp 272−318. Brown, W.; Nicolai, T. *Colloid Polym. Sci.* **1990**, *268*, 977.
(12) Berry, G. C. *Adv. Polym. Sci.* **1994**, *114*, 233.
(13) Fytas, G.; Patkowski, A.; Meier, G.; Dorfmuller, T. *Macromolecules* **1982**, *15*, 870.
(14) Fytas, G.; Patkowski, A.; Meier, G.; Dorfmuller, T. *J. Chem. Phys.* **1984**, *80*, 2214.
(15) Meier, G.; Fytas, G.; Dorfmuller, T. *Macromolecules* **1984**, *17*, 957.

(16) Smith, S. W.; Freeman, B. D.; Hall, C. K. *Macromolecules* **1997**, *30*, 2052.
(17) Kiepen, F.; Borchard, W. *Makromol. Chem.* **1988**, *189*, 2595.
(18) Steinhoff, B.; Rullmann, M.; Kuhne, L.; Alig, I. *J. Chem. Phys.* **1997**, *107*, 5217.
(19) Xiong, Y.; Kiran, E. *Rev. Sci. Instrum.* **1998**, *69*, 1463.
(20) Lechner, M. D.; Mattern, R. *Makromol. Chem.* **1991**, *123/124*, 45.
(21) Szydlowski, J.; Rebelo, L. P.; Van Hook, W. A. *Rev. Sci. Instrum.* **1992**, *63*, 1717.
(22) We recognize that the present data are for polymer solutions at near-critical concentration and high scattering intensity. At low intensity it may well be necessary to continue to use RI matching.
(23) Yaws, C. L., Ed. *Handbook of Viscosity*; Gulf Publ. Co.: Houston TX, 1995.
(24) Tanaka, Y.; Hosakawa, H.; Kubota, H.; Makita, T. *Int. J. Thermophys.* **1991**, *12*, 245.
(25) Bridgeman, P. W. *The Physics of High Pressure;* G. Bell and Sons: London, 1958.
(26) Rabinovitch, I. B. *Influence of isotopy on the physicochemical properties of liquids*; Consultants Bureau: New York, 1970.
(27) de Gennes, P. G. *Scaling concepts in polymer physics*; Cornell University Press: Ithaca, NY, 1979.
(28) Brochard, F.; de Gennes, P. G. *Macromolecules* **1977**, *10*, 1157.
(29) Adam, M.; Delsanti, M. *Macromolecules* **1985**, *18*, 1760.
(30) Semenov, A. N. *Physica A* **1990**, *166*, 263.
(31) Doi, M.; Onuki, A. *J. Phys. II. Fr.* **1992**, *2*, 1631.
(32) Genz, U. *Macromolecules* **1994**, *27*, 3501.
(33) Sun, Z.; Wang, C. H. *Macromolecules* **1994**, *27*, 5667.
(34) Van Hook, W. A.; Wilczura, H.; Imre, A.; Rebelo, L. P. N.; Melnichenko, Y. B.: *Macromolecules* **1999**, *32*, 7312.
(35) Kawasaki, K. *Ann. Phys.* **1970**, *61*, 1. Kawasaki, K.; Lo, S. *Phys. Rev. Lett.* **1972**, *29*, 48.
(36) Stepanek, P. In *Dynamic Light Scattering. The method and some applications*; Brown, W., Ed.; Clarendon Press: Oxford, England, 1993; Chapter 14.
(37) Ikier, C.; Klein, H.; Woermann, D. *Macromolecules* **1995**, *28*, 1003.
(38) Matsuo, S.; Van Hook, W. A. *J. Phys. Chem.* **1984**, *88*, 1032.
(39) Saeki, S.; Kuwahara, N.; Nakata, M.; Kaneko, M. *Polymer* **1975**, *16*, 445.
(40) Ham, J. S.; Bolen, M. C.; Hughes, J. K. *J. Polym. Sci.* **1962**, *57*, 25.
(41) Wolf, B. A.; Geerissen, H. *Colloid Polym. Sci.* **1981**, *259*, 1214.
(42) Imre, A.; Melnichenko, G.; Van Hook, W. A. *Phys. Chem. Chem. Phys.* **1999**, *1*, 4287.
(43) Imre, A.; Melnichenko, G.; Van Hook, W. A. *J. Polym. Sci., Polym. Phys.* **1999**, *37B*, in press.
(44) Vanhee, S.; Kiepen, F.; Brinkmann, D.; Borchard, W.; Koningsveld, R.; Berghmans, H. *Macromol. Chem. Phys.* **1994**, *195*, 759.
(45) Enders, S.; de Loos, Th. W. *Fluid Phase Equilib.* **1997**, *139*, 335.
(46) Hosokawa, H.; Nakata, M.; Dobashi, T. *J. Chem. Phys.* **1993**, *98*, 10078.
(47) Wells, P. A.; de Loos, Th. W.; Kleintjens, L. A. *Fluid Phase Equilib.* **1995**, *106*, 185.
(48) Narayanan, T.; Kumar, A. *Phys. Rep.* **1994**, *249*, 135.
(49) Schneider, G. M. *Ber. Bunsen-Ges. Phys. Chem.* **1972**, *76*, 325. *J. Chem. Thermodynamics* **1991**, *23*, 301.
(50) Prigogine, I.; Defay, R. *Chemical Thermodynamics*; Longmans Green: London, 1954. Translated by Everett, D. H. (Chapter 17).
(51) Rice, O. K. *Chem. Rev.* **1949**, *44*, 65.
(52) Griffiths, R. B.; Wheeler, J. C. *Phys. Rev.* **1970**, *A2*, 1047.
(53) For MW's in the present investigation $P_{hyp}{}^{L}$ lies at a moderate negative pressure and may be located by smoothing data from Table 2, Supporting Information, and the literature (*loc. cit.*). We find $P_{hyp}{}^{L} = (P/\text{MPa}, T/°\text{C}, M_w/\text{solvent}) = \sim(-15, 67, 3 \times 10^4/\text{MCH})$ and $\sim(-10, 87, 2 \times 10^6/\text{MCH})$, for samples of present interest. The curves given in Figures 5a and 6a are not forced through these points in order to allow more precise fitting near $T_{hyp}{}^{L}$ where most of the data lie.
(54) Venkatachalam, S.; Kumar, A.; Gopal, E. S. R. *J. Chem. Phys.* **1995**, *103*, 6645.
(55) Jaffar, B. M.; Venkatachalam, S.; Kumar, A. *Pramana—J. Phys.* **1997**, *49*, 493.
(56) Imre, A.; Van Hook, W. A. Manuscript in preparation.
(57) LeGuillou, J. C.; Zinn-Justin, J. *J. Phys. (Paris)* **1989**, *50*, 1365.
(58) Fetters, L. J.; Hadjichristidis, N.; Lindner, J. S.; Mays, J. W. *J. Phys. Chem. Ref. Data* **1994**, *23*, 619.

MA990238B